Per-Residue Footprints Guided Pharmacophore Model and Pharmacokinetic Profiles for the Discovery of Potential METTL3 Inhibitors Against Myeloid Leukemia

Samukelisiwe Minenhle Mncube
University of KwaZulu-Natal

Abdul Rashid Issahaku
University of KwaZulu-Natal

Mahmoud E. S. Soliman
soliman@ukzn.ac.za

University of KwaZulu-Natal

Research Article

Additional Declarations: No competing interests reported.

Abstract

The impact of the protein METTL3 on tumorigenesis is well-established in cancer research. It promotes cell growth, invasion, migration, and drug resistance. METTL3 is also involved in the modulation of hematopoietic stem cell differentiation. Inhibiting METTL3 presents a potential therapeutic strategy for myeloid leukemia.

This study aimed to identify METTL3 inhibitors through a structure-based virtual screening approach, utilizing an in-house per-residue decomposition virtual screening protocol. We mapped the binding interaction profile of V22, a recognized METTL3 inhibitor, to construct a pharmacophore model for the systematic exploration of potential inhibitors within a chemical database. Four out of nine hit compounds retrieved from ZINC compounds database, showed promising results, and were further investigated.

A comprehensive evaluation of the ADMET properties and physicochemical characteristics of these compounds revealed superior qualities compared to V22. Molecular dynamics (MD) trajectory analysis unveiled substantial structural conformational changes induced by these compounds within the METTL3 protein, offering potential insights into therapeutic inhibition. After mapping per-residue interaction footprints and examining toxicity profiles, we successfully identified the critical residues essential for activity and selectivity, informing our inhibitor design. Furthermore, the four compounds exhibited total binding energies of − 45.3 ± 3.3, − 40.1 ± 4.2, − 56.9 ± 3.3, and − 50.1 ± 4.1 kcal/mol for ZINC67367742, ZINC76585975, ZINC76603049, and ZINC76600653, respectively.

The structural changes observed in proteins upon binding to specific compounds have important therapeutic implications. These alterations include increased stability, improved structural alignment, reduced flexibility, and greater compactness. These changes make these compounds promising candidates for developing more effective therapeutic inhibitors in the treatment of myeloid leukemia.

1. Introduction

N6-methyladenosine (m^6A) is a vital chemical modification of nucleobases that plays a crucial role in regulating gene expression at various levels [1]. Occurring at the N6 position of adenosine, m^6A modification is an abundant internal RNA alteration [1].Among its many functions, m^6A methyltransferase controls several aspects RNA metabolism such as splicing, stability, translation, and localisation.

This modification exerts regulatory control over gene expression by modulating various aspects of mRNA metabolism, encompassing pre-mRNA processing, degradation, nuclear export, and translation. Central to this regulatory mechanism is the protein methyltransferase 3 (METTL3), which not only catalyses m^6A modification but also assumes a pivotal role in cancer biology. METTL3 involvement extends to promoting cancer progression, invasion, survival, metastasis, and drug resistance by modulating the expression of oncogenes and tumor suppressors, employing both m^6A-dependent and independent mechanisms. Moreover, METTL3 participates in shaping the cancer micro-environment such as angiogenesis and immune evasion. Consequently, METTL3 emerges as a prospective therapeutic target for cancer treatment [2].

One hematopoietic malignancy directly linked to METTL3 dysregulation is Acute Myeloid leukemia (AML), characterized by the infiltration of bone marrow, blood and other tissues by proliferative hematopoietic cells [3, 4]. Hematologic malignancies are classified into various categories including myeloid, lymphoid, mixed myelo-lymphoid and dendric neoplasms [5]. Myeloid neoplasms are further grouped into chronic, and acute forms based on the percentage of bone marrow infiltration by immature blasts cells. Chronic myeloid leukemia results from the translocation of chromosome 9 and 22 in hematopoietic stem cells, resulting in activation of BCR-ABL1 kinase and subsequent leukemia stem call formation. Conversely, AML stems from the enlarged proliferation and impaired differentiation of myeloid blasts cells [5].

Consequently, various therapies, including gemtuzumabozogacin, midostaurin, enacidenib, ivosidenib, glasdegib and CPX-351 [6, 7], have been developed and approved for AML treatment. However, challenges such as toxicity [8], mutations leading to resistance [9, 10], and off-target effects [11], underscore the need for more effective and potent alternatives. STM2457 (V22), a highly selective METTL3 inhibitor, has shown promise by suppressing AML growth and facilitating cell differentiation and apoptosis [12]. Despite its potency, V22 awaits regulatory approval [1]. Hence, exploring METTL3 inhibition as a potential strategy for anti-AML therapy is a key focus of our research.

In addition to the classifying myeloid leukemia, comprehending the molecular mechanisms that underlying the disease is imperative. One such mechanism involves post-transcriptional modifications, particularly the role of m^6A modification and its associated enzyme METTL3 in gene expression regulation. N6-methyladenosine modification entails three key of enzymes categories: "writers", "erasers", and "readers" [12]. Writers, including METTL3, METTL5, METTL14, and METTL16, methylate adenine bases on RNA transcripts, with METTL3 and 14 forming a heterodimeric complex [13]. The biological significance of m^6A primarily relies on reader proteins, such as YTHDC1and YTHDC2 which recognizes m^6A-modified sites and direct their interactions with specific cellular locales, thereby modulating processes like mRNA degradation, translation, splicing, stability and export [12]. Erasers, exemplified by FTO predominantly localised in the nucleus, and ALKBH5, present in both the nucleus and cytoplasm, are responsible for removing m^6A modifications from transcripts [14]. Of particular relevance to this study are writer proteins.

The disclosure of the METTL3-METTL14 cocrystals has provided structural insights crucial for designing METTL3 inhibitors [15]. Notable among reported METTL3 inhibitors to date are UZH1a, UZH2, STM2457, and 43n [1, 16, 17]; none of which have progressed to clinical trials. Hence, there exist an urgent need to explore new potential inhibitors candidates to enrich the structural diversity of METTL3 inhibitors.

Numerous endeavours have been undertaken to discover potential METTL3 inhibitors, as discussed recently in a comprehensive review article [18]. Current research endeavours aims to develop METTL3 inhibitors leveraging both functional and structural aspects of the METTL3 domain, with a particular emphasis

on competitively binding of small compounds to the S-adenosyl-L-methionine (SAM) site within METTL3 [19]. This approach led to the emergence of compound V22 as a potent inhibitor of METTL3's catalytic activity, presently undergoing clinical trials [1].

V22 effectively inhibits METTL3-METTL14 catalytic activity with an IC50 of 16.9 nM. Its direct binding to the METTL3-METTL14 heterodimer has been confirmed through surface plasmon resonance (SPR) demonstrating a high affinity of 1.4nM. Operating via a cofactor binding mode, V22 exhibits no disruptive effects on the METTL3-METTL14 complex and displays high specificity for METTL3, with no inhibition observed on other RNA methyltrasferases. These findings indicates that STM2457 is a potent, selective, and readily available inhibitor of METTL3, making it suitable for in vivo studies [1].

Virtual screening has emerged as a pivotal strategy in designing molecular inhibitors for therapeutic targets over the past two decades [20]. Receptor-based or ligand-based virtual screening techniques offer potent in silico tools for identifying novel ligands based on biological structures [21–24]. Consequently, this study is driven by the imperative to strategically identify potential drug candidates for developing new agents targeting myeloid leukemia with inhibitory potential to counteract multidrug resistance. Leveraging the inhibitory efficacy demonstrated by V22 in AML treatment, it is employed as a prototype in our quest for potential METTL3 inhibitors through virtual screening.

2. COMPUTATIONAL METHODS

2.1. Protein preparation

The 3D X-ray crystal structure of METTL3-METTL14 heterodimer in complex with small molecule inhibitor V22 PDB ID: 7O2I, resolution: 3.0 Å [1] was retrieved from RCSB Protein Data Bank. Using UCSF Chimera [24], non-complexing ions and non-standard residues were removed, which involved the removal of chain B (METTL14) and water molecules. Schrodinger Maestro 12.0 software was used to add missing residues. Active site amino acid residues were also defined by using the co-crystallised ligand binding site. Preparing for the MD simulations, the inhibitor, V22, was removed from the structure, and the free protein (unbound) was saved as the receptor in PDB file format (apo). Hydrogen atoms were added to the inhibitor and subsequently saved in Mol2 file format.

2.2. Pharmacophore modeling and virtual screening

Per-residue total energy decomposition evaluation was used to select the residues with high energy contributions to the ligand binding. Residues with energies less than – 1.5 kcal/mol were identified and selected, and their interactions with the components on the V22 ligand were used for pharmacophore development. The designed pharmacophore model was utilized to screen the ZINC library to identify the compounds that might exhibit a great chance to lead to a drug candidate. ZINCPharmer pharmacophore search engine (http://zincpharmer.csb.pitt.edu/) was used to generate a dataset and to screen chemical libraries for molecules that match the ligand's selected components [25]. This tool is a web interface for exploring purchasable compound molecules of the ZINC database utilizing the pharmacophore search technology [25]. The molecular docking technique was then utilized to further sort the selected hit compounds since improper binding of the ligand may indicate various side effects in the body with high chances of toxicity [26]. The known ligand, V22, was re-docked to ensure that the docking program can produce docking poses closer to reality using UCSF Chimera. The atoms in the active site of the protein were defined and displayed through user interfaces. Parameterization was performed where the size of the box was defined, bounding the binding site residues to position the ligand with x= – 7.07108, y=3.41855, and z= 1.20269, for the centre and the size with x=16.1561, y=18.2402, and z=16.9441. The ligand was then docked into the marked active site of the protein. The conformations were displayed in the ViewDock tool in UCSF Chimera [24]. For consistency, the same parameters were utilized to dock all retrieved hits compounds from the library. Inhibitors were also docked using the PyRx open source software [27].

2.3. Molecular dynamics simulations

Molecular dynamics (MD) simulations were conducted by applying the Graphical Processor Unit (GPU) version of Particle Mesh Ewald Molecular Dynamics (PMEMD) integrated into the AMBER18 package [28]. The Antechamber module incorporated in AMBER 18 package was utilized to define force field parameters as well as optimization of the ligand V22 by creating partial charges. The protein and the investigated inhibitors were parameterized utilizing the AMBER force field of 14SB and the general AMBER force field (GAFF), respectively [16, 30].

As well, the pdb4amber incorporated in the AMBER18 package was utilized for the protein preparation. The tleap module in the AMBER18 package was applied to neutralize the complex through the addition of Na^+ and Cl^- counter ions before solvating it with Transferable Intermolecular Potential with 3 points (TIP3P) water box of the size of 10 Å. Topology and parameter files were also created. The created systems were then partially minimized for 2500 steps and then fully minimized with 5000 steps. The systems were gradually heated from 0 to 310 K for 50 ps in moles, volume, and temperature ensemble utilizing a Langevin thermostat at a pressure of 1.0 bar. The systems were then equilibrated for 5 ns at an atmospheric pressure of 1.0 bar utilizing Berendsen barostat [30]. Finally, molecular dynamic production was performed for 500 ns. Generated trajectories and coordinates from the MD productions were analyzed using CPPTRAJ and PTRAJ modules [31] integrated into the AMBER18 package. Origin data analytical tool [32]. Was utilized to plot graphs while snapshots were visualized using BIOVA discovery studio visualizer tool 21.1.0.0. [33].

2.4. Binding affinity calculations

With the aim of predicting the binding free energy of the receptor-ligand complex, we used the Molecular Mechanics Poison-Boltzmann Surface Area (MMPBSA) integrated with the AMBER18 package [28] owing to its extensively reported reliability [34]. The binding energy between the ligand molecule and the receptor protein to form a complex presented in these methods is estimated as follows:

$$\Delta E_{bind} = E_{complex} - (E_{protein} + E_{ligand})$$

$$\Delta G_{bind} = E_{MM} + G_{sol} - T\Delta S$$

Where ΔG_{bind} indicates the free energy of the ligand-protein complex total binding, minus conformational binding entropy (TΔS)

$$\Delta E_{MM} = \Delta E_{int} + \Delta E_{elec} + \Delta E_{vdw}$$

Where ΔE_{MM} shows the total gas phase energy contributed by sum of internal energy, electrostatic and van der Waals energy components. The internal energy indicates the energy that arises from various bonds, angles, c and torque.

$$E_{int} = E_{bond} + E_{angle} + E_{torsion}$$

The sum of the polar $\Delta G_{PB/GB}$ and non-polar ΔG_{SA} contributions to solvation are also represented as follows:

$$\Delta G_{sol} = \Delta G_{PG/GB} + \Delta G_{SA}$$

2.5. Pharmacokinetics and toxicity estimation

ZINC (https://zinc20.docking.org/) was utilized to extract a dataset of the hit compounds to predict drug-likeness. SwissADME (http://www.swissadme.ch/) [35] and ADMETlab2.0 (https://admetmesh.scbdd.com/) [36] were then used to evaluate the pharmacokinetics properties of the selected hit compounds which includes absorption, distribution, metabolism, excretion, and toxicity (ADMET properties). The toxicity of the compounds was further evaluated by estimating the lethal dosage, LD_{50} in mg/kg weight, using ProTox-II (https://tox-new.charite.de/protox_II/) [37]. Chemical compounds with lower LD_{50} values are hazardous and cause a significant risk compared to the compounds with higher LD_{50}.

3. RESULTS AND DISCUSION

3.1. Docking protocol validation

The accuracy and reliability of molecular docking simulations are critical for predicting the binding modes and affinities of ligands within protein targets. In this study, we validated our docking protocol by employing root-mean-square deviation (RMSD), a widely accepted metric for assessing the similarity between docked and experimentally determined protein-ligand complexes [38]. An RMSD score of 2.0 Å or less is commonly considered indicative of a reliable docking pose, suggesting a close agreement between the predicted and crystallographically resolved structures. To verify the accuracy of our docking approach, we superimposed the docked complex of V22 with the crystallographic structure of the METTL3-V22 complex (PDB ID: 7O2I, resolution: 3.0 Å), and calculated the RMSD using UCSF Chimera.

The re-docked V22 compound exhibited an impressively low RMSD value of 0.14 Å when compared to the crystallographic conformation. This minimal deviation indicates a high level of agreement between the predicted binding pose generated by our docking procedure and the experimentally resolved structure.

This validation step instills confidence in the reliability of our docking protocol, affirming its suitability for subsequent analyses and downstream investigations. It ensures that the predicted binding orientations of potential METTL3 inhibitors, derived from our docking simulations, accurately capture the likely binding modes within the METTL3 active site. Thus, our validated docking protocol serves as a robust foundation for the identification and characterization of novel METTL3 inhibitors through virtual screening and computational modeling approaches.

3.2. V22 binding stabilizes METTL3 domain with resultant structural perturbations

Proteins exhibit dynamic behavior in response to various stimuli, including the binding of small molecules, which can induce structural changes. In this study, we investigated the influence of V22 on the structural dynamics of METTL3 to gain insights into its binding mechanism and effects on protein stability. To assess the structural dynamics, we analyzed the root mean square deviation (RMSD) and root mean square fluctuation (RMSF) of the METTL3 domain, along with hydrophobicity and solvent accessible surface area (SASA) of the binding site. RMSD provides information about the stability of the system relative to the starting protein structure, while RMSF characterizes residual fluctuations in the amino acid sequence, reflecting protein flexibility [39]. Analysis of 500 ns molecular dynamics (MD) simulation trajectories revealed that the unbound METTL3 (apo) exhibited lower stability compared to the METTL3-V22 complex, as indicated by average RMSD values of 2.74 Å and 2.42 Å, respectively. Although both systems maintained average RMSD values below 3.0 Å, suggesting overall stability, the presence of V22 induced further stabilization of the system (Fig. 2A).

Furthermore, RMSF analysis revealed increased residue fluctuations in the METTL3-V22 complex compared to the unbound protein, with average RMSF values of 14.98 Å and 15.58 Å, respectively (Fig. 1B). This observation suggests that the binding of V22 enhances the flexibility of the protein structure, potentially facilitating its functional dynamics [40], [41]. Additionally, we probed the hydrophobicity of the binding site to elucidate the effects of V22 binding on local structural properties, although detailed results are not provided here.

Overall, our findings indicate that V22 binding stabilizes the METTL3 domain while inducing structural perturbations characterized by increased residue fluctuations. These insights contribute to a deeper understanding of the molecular interactions underlying METTL3 inhibition and provide valuable information for the rational design of novel inhibitors with improved therapeutic efficacy.

Hydrophobicity, a fundamental property of amino acids, plays a pivotal role in protein stability and folding. It reflects the affinity of amino acid side chains for water, with nonpolar side chains exhibiting higher hydrophobicity compared to polar or charged side chains (Fig. 2).

The hydrophobicity effect is crucial for the stabilization and folding of the protein structure [42]. In our study, hydrophobicity analysis of the binding site provided insights into the structural characteristics crucial for stabilizing the protein structure. As depicted in Fig. 2, the hydrophobicity scale ranged from negative (−3.0) to positive values, with residues in the negative range (blue) being less hydrophobic, and those in the positive range (brown) characterized as

highly hydrophobic. Residues such as Phe534, Leu409, Ile378, Pro397, and the aliphatic portion of the side chain of Arg536 exhibited high hydrophobicity in the brown region, contributing significantly to the surface functionality. These hydrophobic residues are known to possess strong binding affinity with V22, as corroborated by subsequent investigations.

Furthermore, our analysis revealed a spatial distribution of hydrophobicity within the binding pocket, with residues located deeper in the pocket exhibiting higher hydrophobicity (brown) compared to those in the outer regions, which were more hydrophilic (blue). This observation underscores the importance of hydrophobic interactions in stabilizing the protein-ligand complex. Additionally, we assessed the solvent accessible surface area (SASA) of the binding site, another crucial parameter influencing protein folding and stability [43]. SASA impacts surface area minimization, side chain packing density, and burial of hydrophobic side chains. The degree to which residues interact with the solvent and the core is proportional to the surface area exposed to these environments [44]. Residues exposed to solvent interactions (blue) exhibited higher SASA, while those buried within the protein core (green) displayed lower SASA, indicating limited solvent exposure (Fig. 2). Overall, our hydrophobicity and SASA analyses provide valuable insights into the structural features governing protein-ligand interactions. Understanding these characteristics enhances our comprehension of the molecular mechanisms underlying METTL3 inhibition and aids in the rational design of novel inhibitors with improved therapeutic efficacy.

3.3. V22 Binding Interactions within the binding pocket

The binding of a drug molecule or ligand to a specific receptor site is crucial for eliciting therapeutic effects, but improper binding may lead to adverse side effects, including cytotoxicity [26]. In this study, we investigated the interactions between the reference compound V22 and the binding site residues of METTL3 over a simulation period of 500 ns to elucidate the molecular mechanisms underlying their binding dynamics. Analysis of snapshots generated at distinct frames of the simulation revealed that V22 formed multiple types of bonds with the active site residues of METTL3. However, not all interactions persisted throughout the simulation period; some bonds underwent alterations or disappeared entirely as observed in Fig. 3. The sp2 hybridized OD1 atom of Asp395 formed salt bridges with NH_2 atom of V22, while the sp2 hybridized O atom of Pro396 consistently engaged in conventional hydrogen bonding (H-acceptor) with the NH_2 atom of V22. These interactions remained stable throughout the MD simulation period, as depicted in Fig. 3.

The sp2 hybridized O atom in Pro405 only formed conventional hydrogen (H- acceptor) bond at 300 ns, while the O atom of Ser511 formed a carbon-hydrogen bond (H-acceptor) with the ligand through H and NH_2 throughout the simulation time. The sp2 hybridized OE1 atom of Gln550 interacted with the H atom of V22 via a conventional carbon-hydrogen bond (H-acceptor) with a distance of less than 3.5 Å.

Furthermore, the interaction between Thr408 and V22 transitioned from a conventional hydrogen bond to van der Waals forces at 200 ns, reverting back to carbon-hydrogen bonds thereafter. Similarly, Leu409 formed a carbon-hydrogen bond with V22 at 300 ns, while the interaction between Phe534 and V22 persisted through carbon-hydrogen bonds until 400 ns, transitioning back to conventional carbon-hydrogen bonding at 500 ns. Arg436 displayed diverse interactions with V22, including π sigma, π cation, van der Waals, and π alkyl bonds at different time points during the simulation. Additionally, van der Waals forces were observed on non-contact residues.

Overall, our findings highlight the dynamic nature of V22 binding interactions within the METTL3 binding pocket over the simulation period. Understanding these dynamic interactions provides valuable insights into the molecular mechanisms underlying METTL3 inhibition, which may inform the rational design of more effective inhibitors with reduced cytotoxicity and improved therapeutic outcomes.

These observations from the snapshots were supported by computing the hydrogen bond occupancy of the interactions. Since snapshots are a representation of what occurred at a specific frame of the simulation trajectory, this allowed us to ascertain the percentage of the 500 ns simulation occupied by the hydrogen bonds and their average distances. The results are presented in Table 1. As observed, Pro396, and Pro405 are among the residues that formed hydrogen bonds with V22 that endured longer over the simulation period.

H-Acceptor	H-Donor	Occupancy (%)	Average Distance (Å)
Asp395-OD1	V22-H$_2$	92.	2.72
Pro396-O	V22-HN$_2$	84.03	2.81
Pro405-O	V22-H$_1$	18.87	2.82
Asp395-OD1	V22-NH$_2$	3.90	2.78
V22-O1	Gly407-H	27.70	2.87
V22-O	Gly407-H	2.45	2.89
Ser511-O	V22-H$_2$	2.07	2.84
Gln1550-OE1	V22-H	1.79	2.84
V22-O	Asn549-HD21	1.7	2.86
Pro396-O	V22-H$_2$	0.66	2.83
Ser511-O	V22-HN$_2$	0.65	2.82
Gly407-O	V22-H1	0.36	2.81
V22-O	Gln550-HE21	0.24	2.87
Gln550-OE1	V22-H1	0.22	2.81

3.4. Quantitative insights Per-Residue Binding Contribution Towards V22

Decomposing total free binding energies into individual contributions by residues offers insights into the basic nature of the interactions [45]. Binding free energy prediction provides knowledge on the prominent contributors in the interactions between receptor and the ligand. According to Wang, 2018, Molecular Mechanics Poisson-Boltzmann Surface Area (MMPBSA) method is an effective and sensible estimation for free energy simulations due to various key approximations used [46]. Therefore, it can be applied to the evaluations of binding affinities of small molecule ligands bound to a large receptor as a result, it has been used in several studies [35, 49, 51] Furthermore, it provides data on the stability of the complex.

Per-residue energy decomposition (PRED) analysis was conducted to estimate the energy contributions of the individual binding site amino acids toward the total binding energy of V22. It was estimated based on the total energies from electrostatic, van der Waals, polar solvation, and nonpolar solvation energies, and the residues with high total energy contributions were selected. Those with binding energies lower than − 1.5 kcal/mol were considered.

The energy contributions of the individual residues in the binding site, as computed by the decomposition of the total binding energy of the complex, are shown in Fig. 4. Residues that contributed significantly towards the formation of METTL3-V22 are Phe534 (−3.9 ± 0.6 kcal/mol), Pro397 (−3.9 ± 0.4 kcal/mol), Asp395 (−3.3 ± 1.0 kcal/mol), Ser511 (−2.9 ± 0.6 kcal/mol), Ille 378 (−2.1 ± 0.2 kcal/mol), and Arg536 (−1.7 ± 1.0 kcal/mol). In addition, we also assessed the functional groups of the ligand with which these amino acid residues interact.

3.5. Virtual screening and molecular docking

Virtual screening has shown to be a crucial tool in finding small molecule inhibitors that bind to the target receptor [50]. To search for small molecules which have the potential to inhibit the activity of METTL3 compared to the V22, the pharmacophore model in Fig. 5 below was developed and used as a 3D query compound to virtually screen the ZINC database. The model was generated based on the context of the per residue energy decomposition footprint approach where known features from the high contributing amino acid residues (Fig. 4). According to virtual screening results, 9 hit compounds were obtained, and these compounds were then subjected to molecular docking. Four compounds out of nine compounds that exhibited relatively equal or lower docking scores compared to the crystallographic ligand V22 were selected for further analysis.

3.6. Docking of the hit compounds

The docking scores by PyRx virtual screening software for the hit compounds into the target protein are presented in Table 6. Among all the hit compounds, 4 hit compounds with relatively compatible binding scores were selected for further analysis. ZINC67367742, ZINC76585975, ZINC76600653, and ZINC76603049 demonstrated good dock scores with values of − 10.0, − 9.1, − 9.1, − 9.1 kcal/mol, respectively, compared to the crystallographic V22 ligand (calc. − 9.1 kcal/mol) (Table 2). After we ascertained docking scores, we then characterized the physiological properties of the selected compounds. As well, the 2D structures of the selected compounds and the RMSD values of their poses in comparison to V22 after docking are illustrated in Fig. 6. Interestingly the compared poses have structural similarities, especially the amidic bond in all of them.

Table 2
Computed docking scores by UCSF Chimera and PyRx software

Compound	Chimera Docking Score (kcal/mol)	PyRx Docking Score (kcal/mol)
ZINC67367742	−8.7	−10.0
ZINC76585975	−8.3	−8.6
ZINC76600653	−8.3	−9.0
ZINC76603049	−8.3	−9.1
V22	−9.0	−9.1

3.7. Hit compounds induce structural conformational changes to METTL3 upon binding

Molecular dynamics (MD) simulations offers insights into the time-dependent behaviour of the molecular target system at the atomic level [51]. In our study, MD simulations were employed to investigate the conformational changes in the protein structure upon binding of the selected hit compounds. To assess the stability of the compounds within the binding site over the course of a 500 ns simulation period, several metrics were utilized, including root mean square deviation (RMSD), root mean square fluctuation (RMSF), and radius of gyration (RoG) at Cα atoms.

RMSD analysis was performed to evaluate the stability of each compound in the binding site throughout the simulation period. This metric provides insights into the deviation of the compound's position relative to its initial conformation. Figure 7 illustrates the RMSD profiles of the compounds, allowing us to discern their stability within the binding site over time. It is observed that the METTL3 underwent conformational changes due to the binding of the hit compounds. Free METTL3 (apo) displayed an average RMSD of 2.74 Å. In contrast, complexed systems displayed average RMSD values of 2.42 Å for V22; 2.55 Å for ZINC67367742; 2.66 Å for ZINC76603049; 1.95 Å for ZINC76600653; and 3.22 Å for ZINC76585975. ZINC76600653 system showed the least RMSD value compared to other systems, including free METTL3 protein, suggesting it induced the highest stability of METTL3, while ZINC76585975 induced the lowest stability over the simulation period. To accurately reflect the dynamic changes of the METTL3 structures over time, protein structure superimposition was conducted (Fig. 7).

The average of the coordinate differences was calculated for all the atoms in the structures as the measure of similarity of the structures at the period simulation. Superimposition of V22 in complex with METTL3 with reference to free apo yielded RMSD of 1.034 Å. ZINC76585975-, ZINC76600653-, ZINC76603049-, and ZINC67367742- METTL3 complexes displayed an average RMSD of 1.139, 1.012, 1.25, and 1.005 Å, respectively. This alignment of all atoms resulted in a decreased fit with significantly high RMSD values compared to backbone RMSD, as shown in Fig. 7. Probing further to the dynamic changes, RMSF was then conducted.

In addition to RMSD, RMSF analysis was conducted to examine the flexibility of the protein structure upon compound binding. RMSF measures the fluctuation of individual residues within the protein, providing valuable information about dynamic behavior. The parts of the structure with high RMSF values constantly diverge from the average, indicating high flexibility. ZINC76585975 system showed to have least average RMSF value of 12.82 Å in comparison to ZINC76600653, ZINC76603049, ZINC67367742, and V22 systems with RMSF average values of 15.38, 15.87, 15.17, and 14.98 Å, respectively. The unbound apo protein has an average RMSF value of 14.98 Å, which is relatively lower than other systems except for the ZINC76585975 system, which indicated lower residue fluctuations throughout MD simulation. This implies that the molecular flexibility of METTL3 decreased upon binding of ZINC76585975 in the active site. As observed in Fig. 7, the amino acids at 100−120 position displayed the highest mobilities.

The molecular spatial packing of residues is a crucial aspect of protein stability. As such, we computed the RoG of the C_α atoms to ascertain the impact of compound binding on the compactness of the protein. This metric is indicative of the protein structure compactness. The RoG obtained from the MD simulation period revealed less packing density in the 4 systems compared to the free protein due to the relatively high RoG in the complex systems. ZINC76600653, which had the lowest RMSD, displayed the highest compactness amongst the complexed systems with an average RoG value of 16.90 Å in comparison to 17.18 for V22; 17.26 for ZINC76585975; 17.20 for ZINC76603049, and 16.95 Å for ZINC67367742. While the free apo protein exhibited an average RoG of 16.86 Å, which is relatively lower than the other systems. Thus, the stable, least flexible, and compact system among them all was the ZINC76600653 complex system. Due to the stimuli responsiveness of proteins, these characteristics and induced changes could be the starting point towards achieving better therapeutic inhibition. Furthermore, the impacts of the dynamic changes were investigated at the atomic level as the binding site bind to each compound.

3.8. Thermodynamics profile of hit compounds

The binding energy of the complexes was also investigated to compare the binding energies and stability of the complexes using MMPBSA. The change in the binding energy of a mechanism indicates the effects of enthalpy and entropy to estimate whether or not the mechanism is energetically favorable High binding energies suggest favorable energetic interactions [52]. The binding energies were averaged and presented in Table 3. V22 showed average binding energy ($\Delta G_{binding}$) of − 53.0 ± 4.1 kcal/mol against ZINC76603049, ZINC76600653, ZINC67367742, and ZINC76585975 which displayed total binding energies ($\Delta G_{binding}$) of − 56.9 ± 3.3, − 50.1 ± 4.1, − 45.3 ± 3.3, and − 40.1 ± 4.2 kcal/mol, respectively. The calculated binding energies of hit compounds are lower than that of V22 (−53.0 ± 4.1 kcal/mol) except ZINC76603049. The energies presented by the compounds suggest spontaneous complexing of the compounds with METTL3. Van de Waals and electrostatic energies contributed significantly to the total binding energies of the compounds.

Table 3
MMPBSA binding energy profiles of V22, ZINC67367742, ZINC76585975, ZINC76600653, and ZINC76603049 complexed with METTL3.

MMPBSA Binding Energy components (kcal/mol)					
Systems	ΔE_{vdW}	ΔE_{elec}	ΔG_{gas}	ΔG_{sol}	Δ
V22	−63.2 ± 3.9	−142.1 ± 10.0	−205.3 ± 10.1	152.3 ± 9.2	−53.0 ± 4.1
ZINC67367742	−57.3 ± 3.0	−127.8 ± 9.1	−185.0 ± 9.1	139.8 ± 9.0	−45.3 ± 3.3
ZINC76585975	−45.5 ± 2.9	−121.9 ± 14.2	−167.4 ± 14.8	127.3 ± 12.6	−40.1 ± 4.2
ZINC76603049	−57.9 ± 2.6	−145.2 ± 9.0	−203.1 ± 8.9	146.2 ± 8.7	−56.9 ± 3.3
ZINC76600653	−50.4 ± 3.1	−145.8 ± 12.9	−196.2 ± 12.6	146.0 ± 11.3	−50.1 ± 4.1

The stability of a bioactive molecule with an active site is critical for its viable effect [41]. Accordingly, the degree of ligand stability within the binding site of METTL3 was investigated for the simulation period. The average RMSD values of the compounds and V22, which are informative on their stability, are presented in Fig. 8. These results suggest the compounds were generally stable within the binding site. Hit compound molecules in the binding site of METTL3 displayed average RMSD values of 2.50, 1.44, 1.88, and 2.18, for ZINC67367742, ZINC76603049, ZINC76600653, and ZINC76585975 respectively, and 2.24 Å, for V22.

Generally, lower RMSD values regarding actual poses are associated with high binding affinities and represent a good reproduction of the correct pose. Among the inhibitor compounds, ZINC76603049 showed comparatively high stability. There could be potential to use RMSD scores to optimize ligand pose for better orientation and improved binding affinity. From MMPBSA results in Table 3, V22 has a high binding energy while displaying a high RMSD value. Nevertheless, V22 is quite large compared to other hit compounds, giving a great chance of having a high possible number of interactions, possibly more binding modes, and high binding affinity.

3.9. Physiochemical properties and Drug likeness evaluation of hit compounds

An ideal drug should undergo appropriate administration within the body, ensuring effective delivery to various organs and tissues. Moreover, it should be metabolized in a manner that does not immediately compromise its therapeutic activity, while also being eliminated from the body in a timely and safe manner. This comprehensive process encompasses aspects of pharmacokinetics and pharmacodynamics, crucial for ensuring both efficacy and safety of the drug [36]. Lipinski's Rule of Five is a set of criteria used to assess the likelihood of a compound being orally active in humans based on its physicochemical properties. The rule evaluates five key conditions [53]. These criteria encompass molecular weight below 500, estimated octanol-water partition coefficient exceeding 5, fewer than 5 hydrogen bond donors, and fewer than 10 hydrogen bond acceptors [54, 55]. All compounds adhere to Lipinski's rule of five, indicating their potential as biologically active molecules, as demonstrated in Table 4 and Table 7. The partition coefficient (LogP) serves as a descriptor for lipophilicity, representing the relative affinity of a compound for lipid and aqueous phases in its non-ionized state [55]. The hydrophobicity of a ligand contributes to the entropic aspects of molecular interactions, influencing the binding affinity of the ligand-protein complex. Changes in the hydrophobicity of the ligand binding site can lead to alterations in the conformation of the complex [58]. The LogP value serves as an indicator of how a drug should be formulated. As evidenced in Table 4, all four selected hit compounds exhibit LogP values ranging from 1.61 to 2.65, which are lower than the LogP value of V22, which is 3.4. Ideally, drug molecules with LogP values between 1.35 and 1.8 are considered suitable for oral and intestinal absorption. [56].

The size of the drug particles plays a pivotal role in their transport from the gastrointestinal (GI) tract to the active site [57]. Larger particle sizes tend to decrease solubility due to their inverse relationship with surface area [57]. As indicated in Table 4, all compounds possess molecular weights below 500 g/mol, including V22 with a molecular weight of 443.54 g/mol, slightly higher than the selected hit compounds ranging from 326.40 to 386.88 g/mol. This implies their potential for oral distribution.

In conjunction with molecular weight, the count of rotatable bonds significantly impacts both bioavailability and binding efficacy [53]. A rotatable bond is a nonrigid bond connected to a nonterminal, non-hydrogen atom. It is an essential factor in compound permeability since high molecular flexibility causes poor permeability. The number of rotatable bonds of selected hit compounds is nine, making it more flexible than V22 with six rotatable bonds. Also, hydrogen bond donors and hydrogen bond acceptors play a crucial role in the ability of a molecule to permeate the membrane bilayer [58]. A large number of hydrogen bond donor (HBD) groups can reduce a molecule's permeability, while hydrogen bond acceptors (HBA) influence permeability by interconnecting favorably with hydrogen bonding solvents [53]. All selected hit compounds have an HBD of 2, while V22 has an HBD of 3. However, all compounds together with V22 have an HBA of 4. This suggests a good chance of binding potency.

Generally, a well-balanced drug molecule should be adequately hydrophilic to be soluble in aqueous biological fluids and buffer solutions and also adequately lipophilic to penetrate biological membranes [59]. LogS, the logarithm of the molar solubility in water [35] is among the factors affecting absorption. It is the largest concentration of the drug molecule dissolved in the solvent under certain conditions of temperature, pressure and pH [57]. All selected hit compounds including V22 have logS values ranging from − 2.7 to -5.7 l. Compounds with 0 and higher solubility value are highly soluble, those in the range of 0 to − 2 are soluble, those falling within the range of − 2 to − 4 are slightly soluble and insoluble if less than − 4 [60].

The topological surface area (TPSA) molecular descriptor measures the surface area of hetero atoms, nitrogen, oxygen, and their hydrogens [61]. It checks whether the molecule has potential for cell membrane permeability and if a compound possesses > 140 Å^2. ZINC67367742, ZINC76585975, and ZINC76600653 have the STMe TPSA value of 74 Å^2, which is lower than the one observed for ZINC76603049 (79.26 Å^2), which is also lower than that of V22 (91.29 Å^2).

Table 4
Physicochemical properties of the hit compounds selected.

Physiochemical Properties	ZINC67367742	ZINC76585975	ZINC76600653	ZINC76603049	V22
Formula	C20H23ClN4O2	C18H22N4O2	C18H21ClN4O2	C19H27N5O2	C25H29N6O2
MW (g/mol)	386.883	326.4	360.845	357.458	444.53
Log $P_{o/w}$	2.65	1.61	2.20	1.74	3.48
LogS (Ali) (mol/L)	−4.20	−2.70	−3.70	−2.99	−5.77
TPSA ($\text{\AA}^2$)	74.33	74.33	74.33	79.26	91.29
HA	27	24	25	26	33
H-bond acceptors	4	4	4	4	5
H-bond donors	2	2	2	2	4
Rotatable bonds	9	9	9	9	8
Lipinski violations	No; 0	No; 0	No; 0	No; 0	No; 0

3.10. Toxicity of selected hit compounds

In silico toxicity, evaluation is an important method for appropriate lead compound selection before a drug candidate goes through a clinical trial [40]. The toxicity classes are defined by their corresponding LD_{50} values in milligrams per kilogram (mg/kg), specifically focusing on the fatal and toxic ranges. These classes range from "Fatal if swallowed" for LD_{50} values less than or equal to 55 mg/kg, to "Toxic if swallowed" for LD_{50} values between 50 and 300 mg/kg [62]. According to the ProTox II webserver, all selected 4 hit compounds belong to class 4 for acute oral toxicity, where ZINC67367742, ZINC76585975, and ZINC76603049 have the LD_{50} values of 1000 mg/kg, while ZINC76600653 has an LD_{50} value of 590 mg/kg. These would be dangerous if taken orally. However, the predicted median lethal dose associated with the original ligand V22 shows to be more harmful as it belongs to class 4 with LD_{50} value of 250 mg/kg as shown in Table 5.

Table 5
Toxicity of the selected hit compounds.

	ZINC67367742	ZINC76585975	ZINC76600653	ZINC76600653	V22
$\varvec{L}\varvec{D}_{50}$ (mg/kg)	1000 mg/kg	1000 mg/kg	1000 mg/kg	590 mg/kg	250 mg/kg
Toxicity class	Class 4	Class 4	Class 4	Class 4	Class 3

Table 6

Canonical smiles for other hit compounds

Zinc ID	Canonical smile	Chimera Docking Score (kcal/mol)	PyRx Docking Score (kcal/mol)
ZINC67367742	CN1CCN(CC1) c1ccc(cc1) [C@@H] (NC(=O) N[C@H]1CCO[C@H]1C) C	−8.7	−10.0
ZINC76585975	CN(CCc1ccc(cc1) NC(=O) C(=O) N[C@@H] (c1cn(nc1C) C) C) C	−8.3	−8.6
ZINC76600653	CN(CCc1ccc(cc1) NC(=O) C(=O) NCc1ccc(nc1) Cl) C	−8.3	−9.0
ZINC68316170	CN1CCN(CC1) c1ccc(cc1) [C@@H] (NC(=O) N[C@@H]1CCO[C@H]1C) C	−7.8	−8.4
ZINC76158525	CN(CCc1ccc(cc1) NC(=O) C(=O) Nc1c[nH]nc1) C	−8.7	−8.6
ZINC92651254	COc1cccc(c1) OCC(=O) Nc1ccc(cc1) CCN(C)C	−8.4	−8.7
ZINC95448669	Coc1cc (OC)ccc1NC(=O) c1ccnc(c1) N1CCN(CC1) C	−7.7	−8.0
ZINC95448671	Clc1ccc(cn1) CNC(=O) C(=O) Nc1ccc(cc1) CCN1CCCC1	−7.4	−7.9
ZINC76603049	CN(CCc1ccc(cc1) NC(=O) C(=O) NCc1cccnc1) C	−8.3	−9.1

Table 7

Physiological properties of the hit compounds retrieved.

ZINC ID	Formula	Mw (g/mol)	LogP	LogS	TPSA	HBA	HBD	Rotatable bonds	GI	Lipinski Drug likeness
ZINC67367742	C19H30N4O2	346.47	1.71	- 2.49	56.84 A2	3	2	6	High	Yes; 0 violation
ZINC68316170	C19H30N4O2	346.47	1.72	-2.49	56.84 A2	3	2	6	High	Yes; 0 violation
ZINC76158525	C15H19N5O2	301.34	0.95	-2.44	90.12 A2	4	3	8	High	Yes; 0 violation
ZINC76585975	C19H27N5O2	357.45	1.74	-2.99	79.26 A2	4	2	9	High	Yes; 0 violation
ZINC76600653	C18H21ClN4O2	360.84	2.20	-3.70	74.33 A2	4	2	9	High	Yes; 0 violation
ZINC76603049	C18H22N4O2	326.39	1.61	-2.70	74.33 A2	4	2	9	High	Yes; 0 violation
ZINC92651254	C19H24N2O3	328.41	2.79	-3.73	50.80 A2	4	1	9	High	Yes; 0 violation
ZINC95448669	C19H24N4O3	356.42	1.87	-2.93	66.93 A2	5	1	6	High	Yes; 0 violation
ZINC95448671	C20H23ClN4O2	386.88	2.65	-4.20	74.33 A2	4	2	8	High	Yes; 0 violation

3.11. Intermolecular interaction profiling of hit compounds within METTL3 binding pockets.

The impact of compounds on the protein is determined by their interactions, influencing both the binding site and the overall structure of the protein [63]. Analysis of snapshots extracted from molecular dynamics (MD) simulation trajectories of the METTL3-ZINC complexes revealed diverse bonding patterns between the compounds and residues within the binding pocket. These interactions encompassed conventional hydrogen bonds, carbon hydrogen bonds, Van der Waals forces, alkyl interactions, salt bridges, pi-alkyl interactions, pi-cation interactions, pi-sigma interactions, and pi-stacking interactions. While certain interactions remained stable throughout the simulation, others exhibited temporal fluctuations.

Key residues participating in these interactions were identified, including Arg471, Arg536, Thr510, Phe534, Asp395, Tyr406, Pro397, Trp457, Lys459, Val507, Ser511, His512, Lys513, and Trp457, highlighting their crucial role in ligand binding. Visualization of the interaction patterns is provided in Fig. 9 and Fig. 10.

Notably, several interactions observed in the compounds mirror the binding modes observed with the reference compound V22. These similarities suggest a high binding affinity and specificity of the compounds towards METTL3, as they engage multiple residues essential for the catalytic function and substrate recognition of METTL3[64].

Conclusion

In summary, the N6 adenosine methyl transferase catalytic unit (METTL3) stands out as a promising focal point for advancing myeloid leukemia therapy. The quest for METTL3 inhibitors has made significant strides in recent years, with our efforts centered on modeling a pharmacophore based on the structural features of the known inhibitor, V22, through a meticulous per-residue footprint approach. This endeavour yielded nine potential hit compounds following the screening of the ZINC compound database against the pharmacophore model. Notably, ZINC67367742, ZINC76603049, ZINC76600653, and ZINC76585975 displayed robust docking scores alongside favorable physicochemical attributes, indicating their potential as less toxic inhibitors compared to the established V22.

Subsequent molecular docking and dynamics simulations highlighted significant conformational alterations in METTL3 upon interaction with these four compounds. Furthermore, thermodynamic analysis revealed substantial free binding energies, further underlining their promise as METTL3 inhibitors.

While our study significantly enriches our knowledge of available compound molecules with inhibitory potential against METTL3, rigorous experimental validation of these compounds remains imperative to ascertain their efficacy. This validation step not only ensures the reliability of our findings but also sets the stage for potential enhancements aimed at enhancing their inhibitory prowess, thus opening avenues for the development of more potent anticancer agents targeting Myeloid leukemia.

Moreover, a deeper investigation into the inhibitory mechanisms underlying the action of these compounds against METTL3 holds promise for unveiling crucial insights into the nature of inhibition and its potential impact on cellular processes in vivo. Such insights may offer valuable implications for the broader therapeutic landscape of METTL3 inhibition and its implications in combating myeloid leukemia.

Declarations

Conflict of Interest

Authors declare no financial and intellectual conflict of interests.

References

1. Yankova, E.; Blackaby, W.; Albertella, M.; Rak, J.; De Braekeleer, E.; Tsagkogeorga, G.; Pilka, E.S.; Aspris, D.; Leggate, D.; Hendrick, A.G. Small-molecule inhibition of METTL3 as a strategy against myeloid leukaemia. *Nature* **2021**, *593*, 597–601, doi:10.1038/s41586-021-03536-w.

2. Zeng, C.; Huang, W.; Li, Y.; Weng, H. Roles of METTL3 in cancer: Mechanisms and therapeutic targeting. *J. Hematol. Oncol.* **2020**, *13*, 1–15, doi:10.1186/s13045-020-00951-w.

3. Stoner, G.L. Molecular and 2001, *7*, 1115–1139.

4. Pelcovits, A.; Niroula, R. Acute Myeloid Leukemia: A Review. *R. I. Med. J. (2013)* **2020**, *103*, 38–40.

5. Schürch, C.M.; Riether, C.; Ochsenbein, A.F. Dendritic cell-based immunotherapy for myeloid leukemias. *Front. Immunol.* **2013**, *4*, 1–16, doi:10.3389/fimmu.2013.00496.

6. Yamashita, T.; Sakano, T.; Iqbal Mahamood, M.; Fujitani, H. Biophysics and Physicobiology Molecular dynamics analysis to evaluate docking pose prediction. **2016**, *13*, 181–194, doi:10.2142/biophysico.13.0_181.

7. Wei, A.H.; Tiong, I.S. Midostaurin, enasidenib, CPX-351, gemtuzumab ozogamicin, and venetoclax bring new hope to AML. *Blood* **2017**, *130*, 2469–2474, doi:10.1182/blood-2017-08-784066.

8. Manuel, J.; Gervasini, G. Chemotherapy Toxicity in Patients with Acute Leukemia. *Acute Leuk. - Sci. Perspect. Chall.* **2011**, doi:10.5772/21239.

9. Zhang, J.; Gu, Y.; Chen, B. Mechanisms of drug resistance in acute myeloid leukemia. *Onco. Targets. Ther.* **2019**, *12*, 1937–1945, doi:10.2147/OTT.S191621.

10. Yu, J.; Li, Y.; Zhang, D.; Wan, D.; Jiang, Z. Clinical implications of recurrent gene mutations in acute myeloid leukemia. *Exp. Hematol. Oncol.* **2020**, *9*, 1–11, doi:10.1186/s40164-020-00161-7.

11. Steegmann, J.L.; Cervantes, F.; Le Coutre, P.; Porkka, K.; Saglio, G. Off-target effects of BCRABL1 inhibitors and their potential long-term implications in patients with chronic myeloid leukemia. *Leuk. Lymphoma* **2012**, *53*, 2351–2361, doi:10.3109/10428194.2012.695779.

12. Wu, X.; Ye, W.; Gong, Y. The Role of RNA Methyltransferase METTL3 in Normal and Malignant Hematopoiesis. *Front. Oncol.* **2022**, *12*, 1–10, doi:10.3389/fonc.2022.873903.

13. Joshi, K.; Wang, D.O.; Gururajan, A. The m6A-methylome in major depression: A bioinformatic analysis of publicly available datasets. *Psychiatry Res. Commun.* **2022**, *2*, 100089, doi:10.1016/j.psycom.2022.100089.

14. Yankova, E. and D.A. Europe PMC Funders Group The m 6 A RNA modification in AML. **2022**, *28*, 80–85, doi:10.1097/MOH.0000000000000636.The.

15. Wang, P.; Doxtader, K.A.; Nam, Y. Structural Basis for Cooperative Function of Mettl3 and Mettl14 Methyltransferases. *Mol. Cell* **2016**, *63*, 306–317, doi:10.1016/j.molcel.2016.05.041.

16. Du, Y.; Yuan, Y.; Xu, L.; Zhao, F.; Wang, W.; Xu, Y.; Tian, X. Discovery of METTL3 Small Molecule Inhibitors by Virtual Screening of Natural Products. *Front. Pharmacol.* **2022**, *13*, 878135, doi:10.3389/fphar.2022.878135.

17. Moroz-Omori, E. V.; Huang, D.; Kumar Bedi, R.; Cheriyamkunnel, S.J.; Bochenkova, E.; Dolbois, A.; Rzeczkowski, M.D.; Li, Y.; Wiedmer, L.; Caflisch, A. METTL3 Inhibitors for Epitranscriptomic Modulation of Cellular Processes. *ChemMedChem* **2021**, *16*, 3035–3043, doi:10.1002/cmdc.202100291.

18. Fiorentino, F.; Menna, M.; Rotili, D.; Valente, S.; Mai, A. METTL3 from Target Validation to the First Small-Molecule Inhibitors: A Medicinal Chemistry Journey. *J. Med. Chem.* **2023**, *66*, 1654–1677, doi:10.1021/acs.jmedchem.2c01601.

19. Xu, P.; Ge, R. Roles and drug development of METTL3 (methyltransferase-like 3) in anti-tumor therapy. *Eur. J. Med. Chem.* **2022**, *230*, 114118, doi:10.1016/j.ejmech.2022.114118.

20. Sanchez, G. Discovery of binding proteins for a protein target using protein-protein docking-based virtual screeningLas instituciones de ciencia y tecnología en los procesos de aprendizaje de la producción agroalimentaria en Argentina. *El Sist. argentino innovación Inst. Empres. y redes. El desafío la creación y apropiación Conoc.* **2013**, *14*, 659–664, doi:10.1002/prot.

21. Shoichet, B.K. Virtual screening of chemical libraries. **2006**, *432*, 862–865.

22. Ferreira, L.G.; Dos Santos, R.N.; Oliva, G.; Andricopulo, A.D. *Molecular docking and structure-based drug design strategies*; 2015; Vol. 20; ISBN 5516337380.

23. Coelho Santos Junior, M.; Henriques Soares Leal, D.; Habib Bechelane Maia, E.; Cristina Assis, L.; Alves de Oliveira, T.; Marques da Silva, A.; Gutterres Taranto, A. Structure-Based Virtual Screening: From Classical to Artificial Intelligence. *Front. Chem. | www.frontiersin.org* **2020**, *1*, 343, doi:10.3389/fchem.2020.00343.

24. Pettersen, E.F.; Goddard, T.D.; Huang, C.C.; Couch, G.S.; Greenblatt, D.M.; Meng, E.C.; Ferrin, T.E. UCSF Chimera - A visualization system for exploratory research and analysis. *J. Comput. Chem.* **2004**, *25*, 1605–1612, doi:10.1002/jcc.20084.

25. Koes, D.R.; Camacho, C.J. ZINCPharmer: Pharmacophore search of the ZINC database. *Nucleic Acids Res.* **2012**, *40*, 409–414, doi:10.1093/nar/gks378.

26. Opo, F.A.D.M.; Rahman, M.M.; Ahammad, F.; Ahmed, I.; Bhuiyan, M.A.; Asiri, A.M. Structure based pharmacophore modeling, virtual screening, molecular docking and ADMET approaches for identification of natural anti-cancer agents targeting XIAP protein. *Sci. Rep.* **2021**, *11*, 1–18, doi:10.1038/s41598-021-83626-x.

27. Dallakyan, S.; Olson, A.J. Chapter 19 Small-Molecule Library Screening by Docking with PyRx. **2015**, *1263*, 243–250, doi:10.1007/978-1-4939-2269-7.

28. Mermelstein, D.J.; Lin, C.; Nelson, G.; Kretsch, R.; McCammon, J.A.; Walker, R.C. Fast and flexible gpu accelerated binding free energy calculations within the amber molecular dynamics package. *J. Comput. Chem.* **2018**, *39*, 1354–1358, doi:10.1002/jcc.25187.

29. Wang, J.; Wolf, R.M.; Caldwell, J.W.; Kollman, P.A.; Case, D.A. Development and testing of a general amber force field. *J. Comput. Chem.* **2004**, *25*, 1157–1174, doi:10.1002/jcc.20035.

30. Berendsen, H.J.C.; Postma, J.P.M.; van Gunsteren, W.F.; DiNola, a; Haak, J.R. Molecular dynamics with coupling to an external bath. *J. Chem. Phys.* **1984**, *81*, 3684–3690, doi:10.1063/1.448118.

31. Roe, D.R.; Cheatham, T.E. PTRAJ and CPPTRAJ: Software for Processing and Analysis of Molecular Dynamics Trajectory Data. *J. Chem. Theory Comput.* **2013**, *9*, 3084–3095, doi:10.1021/ct400341p.

32. Deschenes, L.A. Origin 6.0: Scientific Data Analysis and Graphing Software Origin Lab Corporation. *J. Am. Chem. Soc* **2000**, *122*, 9566–9570.

33. BIOVIA, D.S. Discovery Studio 2017.

34. Issahaku, A.R.; Aljoundi, A.; Soliman, M.E.S. Establishing the mutational effect on the binding susceptibility of AMG510 to KRAS switch II binding pocket: Computational insights. *Informatics Med. Unlocked* **2022**, *30*, 100952, doi:https://doi.org/10.1016/j.imu.2022.100952.

35. Daina, A.; Michielin, O.; Zoete, V. SwissADME: A free web tool to evaluate pharmacokinetics, drug-likeness and medicinal chemistry friendliness of small molecules. *Sci. Rep.* **2017**, *7*, doi:10.1038/srep42717.

36. Xiong, G.; Wu, Z.; Yi, J.; Fu, L.; Yang, Z.; Hsieh, C.; Yin, M.; Zeng, X.; Wu, C.; Lu, A. ADMETlab 2.0: an integrated online platform for accurate and comprehensive predictions of ADMET properties. *Nucleic Acids Res.* **2021**, *49*, doi:10.1093/nar/gkab255.

37. Banerjee, P.; Eckert, A.O.; Schrey, A.K.; Preissner, R. ProTox-II: a webserver for the prediction of toxicity of chemicals. *Nucleic Acids Res.* **2018**, *46*, W257–W263, doi:10.1093/nar/gky318.

38. Carugo, O. Statistical validation of the root-mean-square-distance, a measure of protein structural proximity. *Protein Eng. Des. Sel.* **2007**, *20*, 33–37, doi:10.1093/protein/gzl051.

39. Aier, I.; Varadwaj, P.K.; Raj, U. Structural insights into conformational stability of both wild-type and mutant EZH2 receptor. *Sci. Rep.* **2016**, *6*, 1–10, doi:10.1038/srep34984.

40. Dain, F.A.; Opo, M.; Rahman, M.M.; Ahammad, F.; Ahmed, I.; Bhuiyan, A.; Asiri, A.M. Structure based pharmacophore modeling, virtual screening, molecular docking and ADMET approaches for identification of natural anti-cancer agents targeting XIAP protein. *Sci. Reports |* **123AD**, *11*, 4049, doi:10.1038/s41598-021-83626-x.

41. Rudrapal, M.; Issahaku, A.R.; Agoni, C.; Bendale, A.R.; Nagar, A.; Soliman, M.E.S.; Lokwani, D.; Rudrapal, M.; Issahaku, A.R.; Agoni, C. In silico screening of phytopolyphenolics for the identification of bioactive compounds as novel protease inhibitors effective against SARS-CoV-2. *J. Biomol. Struct. Dyn.* **2021**, *0*, 1–17, doi:10.1080/07391102.2021.1944909.

42. Karyagina, A.; Ershova, A.; Titov, M.; Olovnikov, I.; Aksianov, E.; Ryazanova, A.; Kubareva, E.; Spirin, S.; Alexeevski, A. Analysis of conserved hydrophobic cores in proteins and supramolecular complexes. *J. Bioinform. Comput. Biol.* **2006**, *4*, 357–372, doi:10.1142/S0219720006001837.

43. Savojardo, C.; Manfredi, M.; Martelli, P.L.; Casadio, R. Solvent Accessibility of Residues Undergoing Pathogenic Variations in Humans: From Protein Structures to Protein Sequences. *Front. Mol. Biosci.* **2021**, *7*, 1–9, doi:10.3389/fmolb.2020.626363.

44. Durham, E.; Dorr, B.; Woetzel, N.; Staritzbichler, R.; Meiler, J. Solvent accessible surface area approximations for rapid and accurate protein structure prediction. *J. Mol. Model.* **2009**, *15*, 1093–1108, doi:10.1007/s00894-009-0454-9.

45. Scheiner, S.; Kar, T.; Pattanayak, J. Comparison of Various Types of Hydrogen Bonds Involving Aromatic Amino Acids. **2002**, doi:10.1021/ja027200q.

46. Wang, C.; Greene, D.; Xiao, L.; Qi, R.; Luo, R. Recent Developments and Applications of the MMPBSA Method. *Front. Mol. Biosci.* **2018**, *4*, doi:10.3389/fmolb.2017.00087.

47. Agoni, C.; Issahaku, A.R.; Abdelgawad, M.A.; Khames, A.; Soliman, M.E.S.; Mathew, B. Extended double bond conjugation in the chalcone framework favours MAO-B inhibition: A structural perspective on molecular dynamics. *Comb. Chem. High Throughput Screen.* **2022**, doi:10.2174/1386207325666220214110717.

48. Issahaku, A.R.; Agoni, C.; Kumi, R.O.; Olotu, F.A.; Soliman, M.E.S. Lipid-Embedded Molecular Dynamics Simulation Model for Exploring the Reverse Prostaglandin D2 Agonism of CT-133 towards CRTH2 in the Treatment of Type-2 Inflammation Dependent Diseases. *Chem. Biodivers.* **2020**, *17*, e1900548, doi:10.1002/cbdv.201900548.

49. Issahaku, A.R.; Salifu, E.Y.; Soliman, M.E.S. Inside the cracked kernel: establishing the molecular basis of AMG510 and MRTX849 in destabilising KRASG12C mutant switch I and II in cancer treatment. *J. Biomol. Struct. Dyn.* **2022**, 1–13, doi:10.1080/07391102.2022.2074141.

50. Koch, G. Medicinal Chemistry. *Chimia (Aarau).* **2017**, *71*, 643, doi:10.2307/j.ctvnwc0d0.18.

51. Singh, S.; Singh, V.K. Molecular Dynamics Simulation: Methods and Application. *Front. Protein Struct. Funct. Dyn.* **2020**, 213–238, doi:10.1007/978-981-15-5530-5_9.

52. Schottel, B.L.; Chifotides, H.T.; Dunbar, K.R. Anion-Π interactions. *Chem. Soc. Rev.* **2008**, *37*, 68–83, doi:10.1039/b614208g.

53. Ivanović, V.; Rančić, M.; Arsić, B.; Pavlović, A. Lipinski's rule of five, famous extensions and famous exceptions. *Pop. Sci. Artic.* **2020**, *3*, 171–177.

54. Waterbeemd, H. Van De 11 Relation of Molecular Properties. **2002**.

55. Bhal, S.K. Understanding When to Use Log P & Log D. *ACD/Labs - Adv. Chem. Dev. Inc. Toronto, Canada.* **2019**, 3–6.

56. K. Bhal, S. Log P — Making Sense of the Value. *Adv. Chem. Dev.* **2007**, 1–4.

57. Gohil, T. Solubility Enhancement of Poorly Water Soluble Drugs. *Indones. J. Pharm.* **2014**, *25*, 1, doi:10.14499/indonesianjpharm25iss1pp1.

58. Objective, L. H-bond donors vs H-bond acceptors Comparing Physical Properties of H-bond Donors vs H- bond Acceptors. **2021**, 1–2.

59. Coltescu, A.R.; Butnariu, M.; Sarac, I. The importance of solubility for new drug molecules. *Biomed. Pharmacol. J.* **2020**, *13*, 577–583, doi:10.13005/BPJ/1920.

60. Sorkun, M.C.; Khetan, A.; Er, S. AqSolDB, a curated reference set of aqueous solubility and 2D descriptors for a diverse set of compounds. *Sci. Data* **2019**, *6*, 1–8, doi:10.1038/s41597-019-0151-1.

61. Prasanna, S.; Doerksen, R.J. Topological polar surface area: a useful descriptor in 2D-QSAR. *Curr. Med. Chem.* **2009**, *16*, 21–41, doi:10.2174/092986709787002817.

62. Drwal, M.N.; Banerjee, P.; Dunkel, M.; Wettig, M.R.; Preissner, R. ProTox: A web server for the in silico prediction of rodent oral toxicity. *Nucleic Acids Res.* **2014**, *42*, 53–58, doi:10.1093/nar/gku401.

63. Issahaku, A.R.; Mukelabai, N.; Agoni, C.; Rudrapal, M.; Aldosari, S.M.; Almalki, S.G.; Khan, J. Characterization of the binding of MRTX1133 as an avenue for the discovery of potential KRASG12D inhibitors for cancer therapy. *Sci. Rep.* **2022**, *12*, 17796, doi:10.1038/s41598-022-22668-1.

64. Śledź, P.; Jinek, M. Structural insights into the molecular mechanism of the m6A writer complex. *Elife* **2016**, *5*, 1–16, doi:10.7554/eLife.18434.
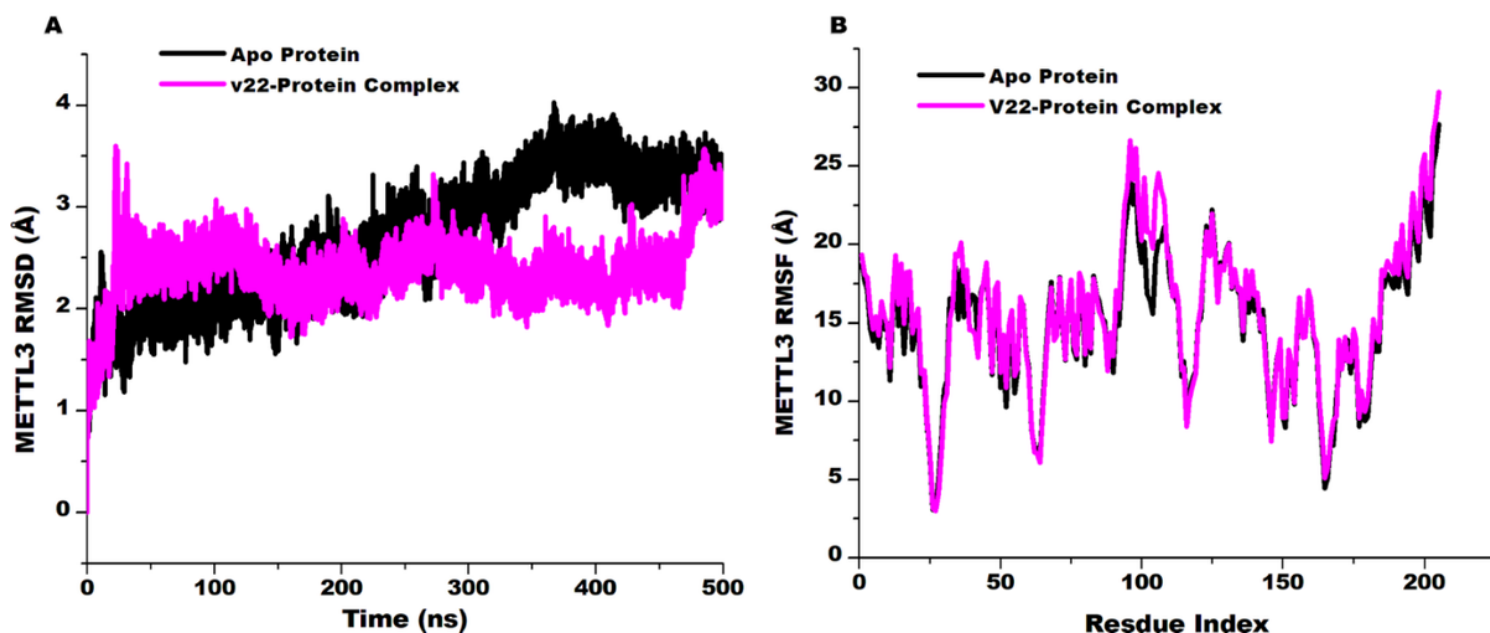
Figures

Figure 1

(A) RMSD plot of C_a atoms and **(B)** RMSF plot of individual amino acid residues of METTL3-V22 complex (in black) in comparison with unbound METTL3 (in pink).
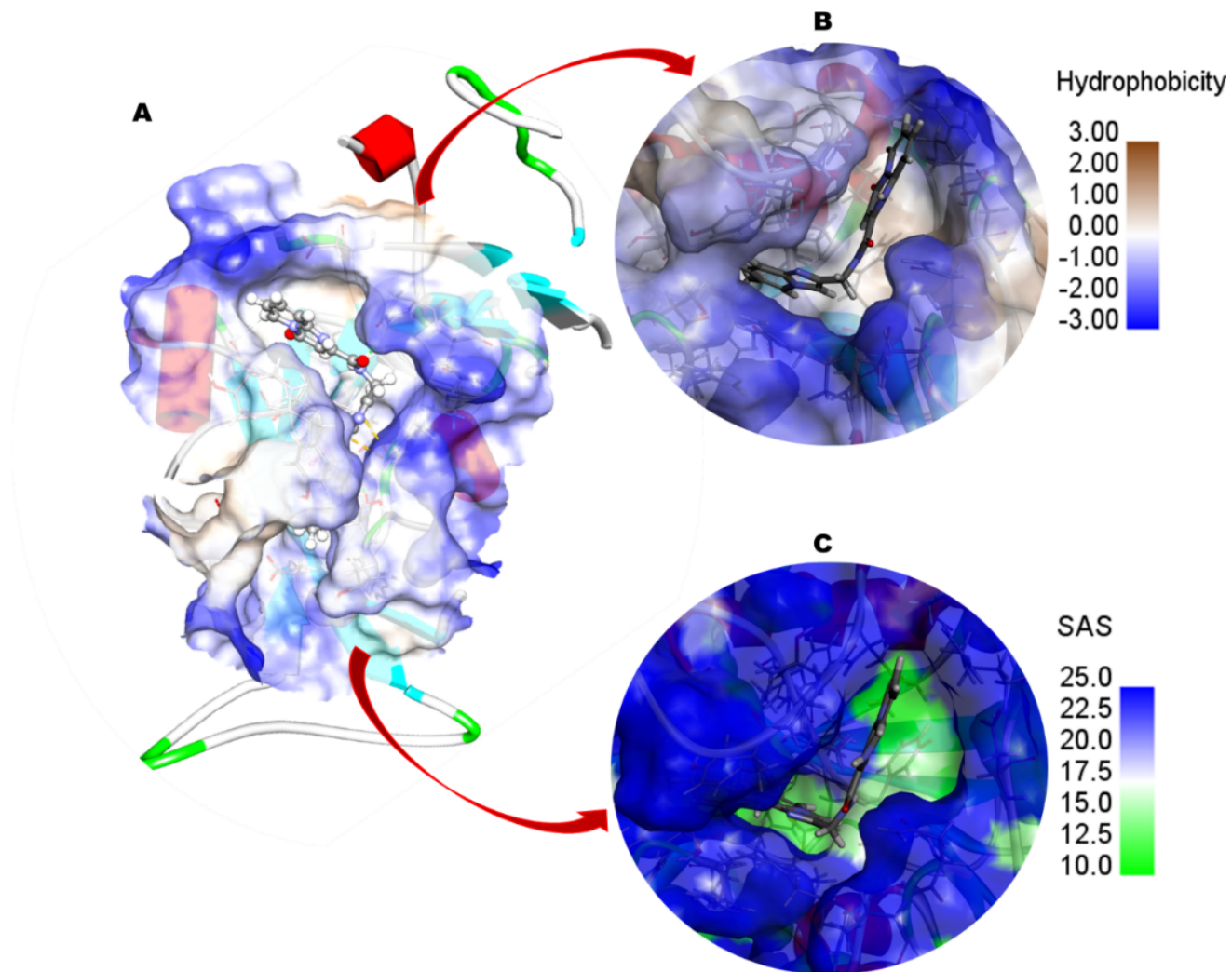
Figure 2

(A)The binding pocket of METTL3, (B) the hydrophobicity of the binding pocket of the V22 bound with METTL3 protein, and (C) the solvent-accessible surface area (SASA) of the binding pocket.
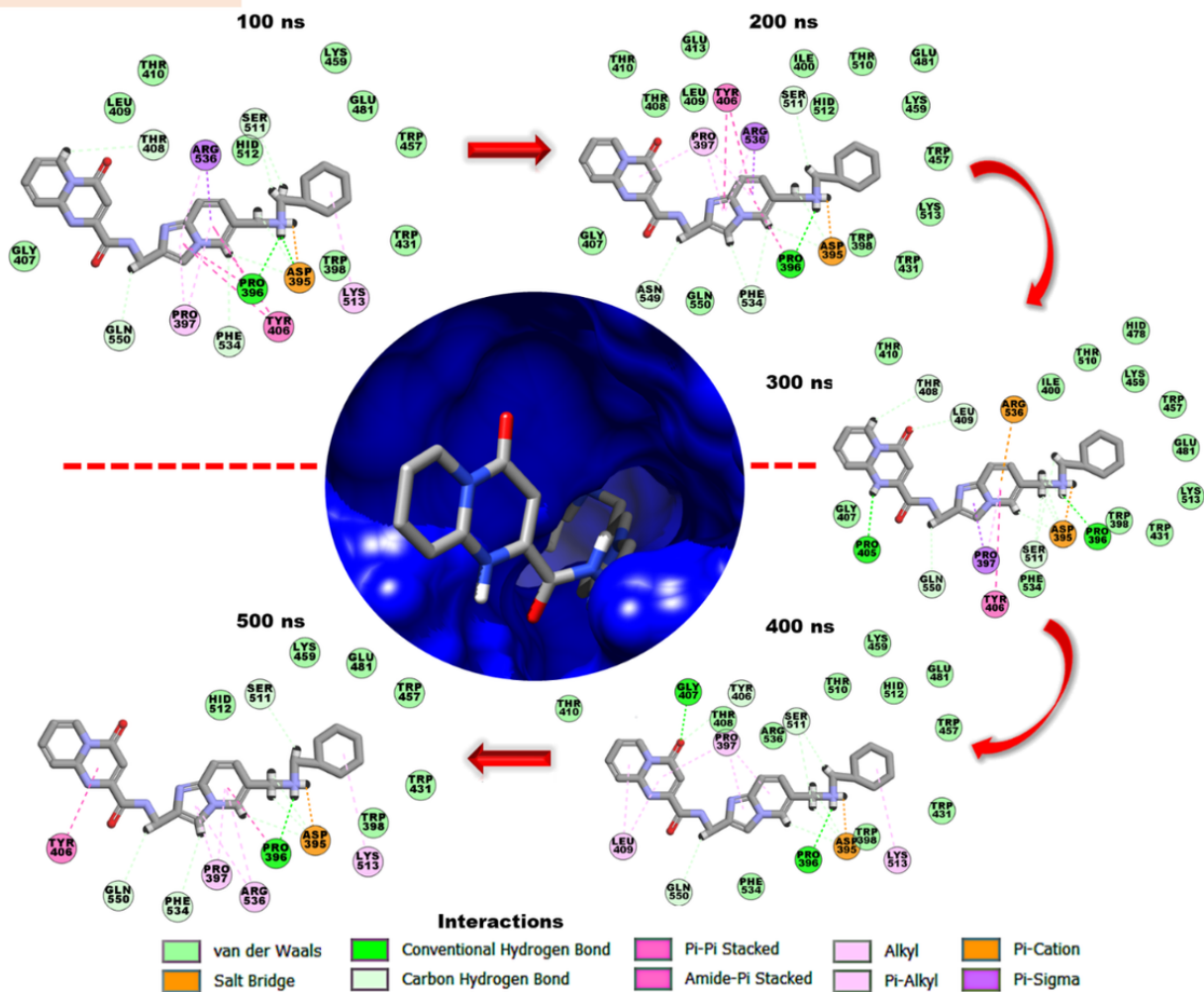
Figure 3

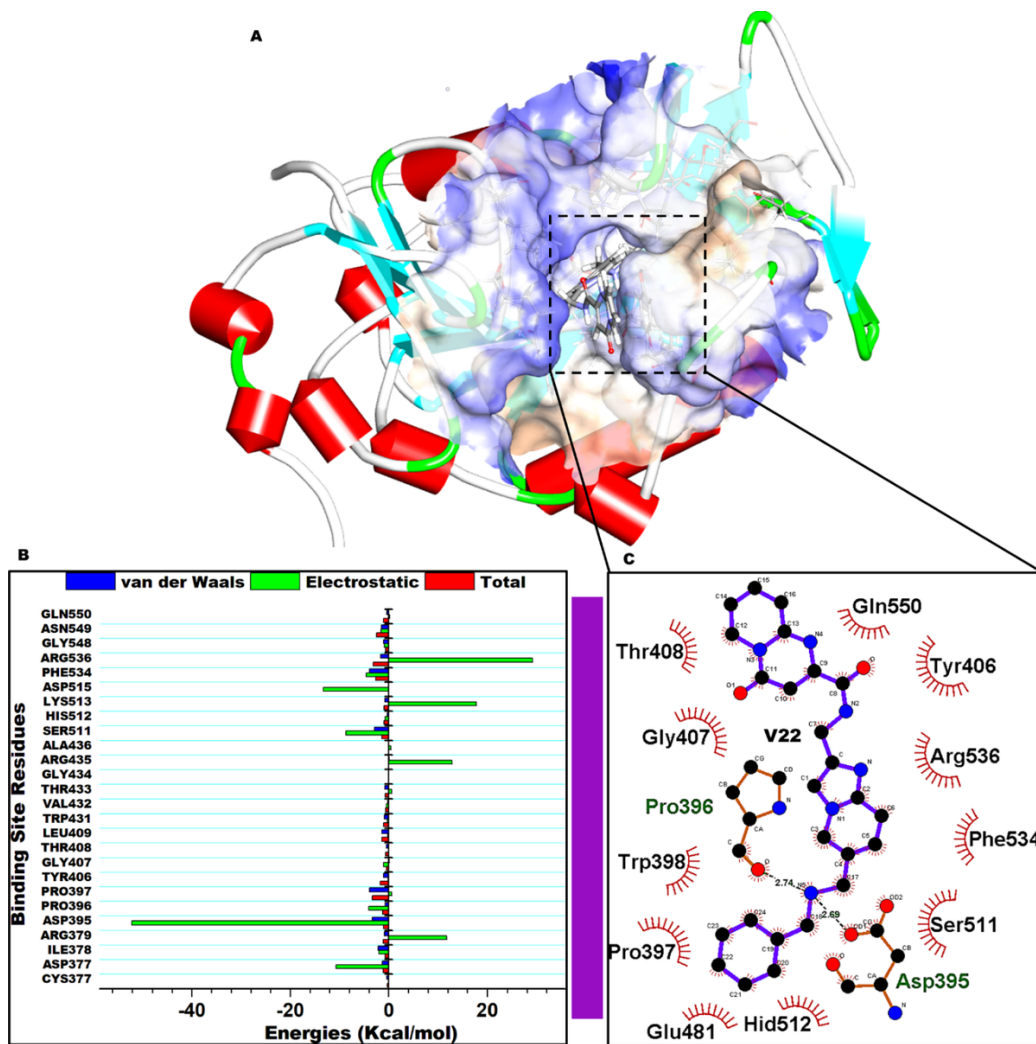Schematic representation of METTL3 interactions with V22 over 100, 200, 300, 400, and 500 ns.

Figure 4

(A) V22 within the binding site of METTL3 protein, (B) Per-residue energy plots of binding sites residues towards V22 complexing with METTL3, and (C) The 2D representation of intermolecular interactions exhibited by V22.
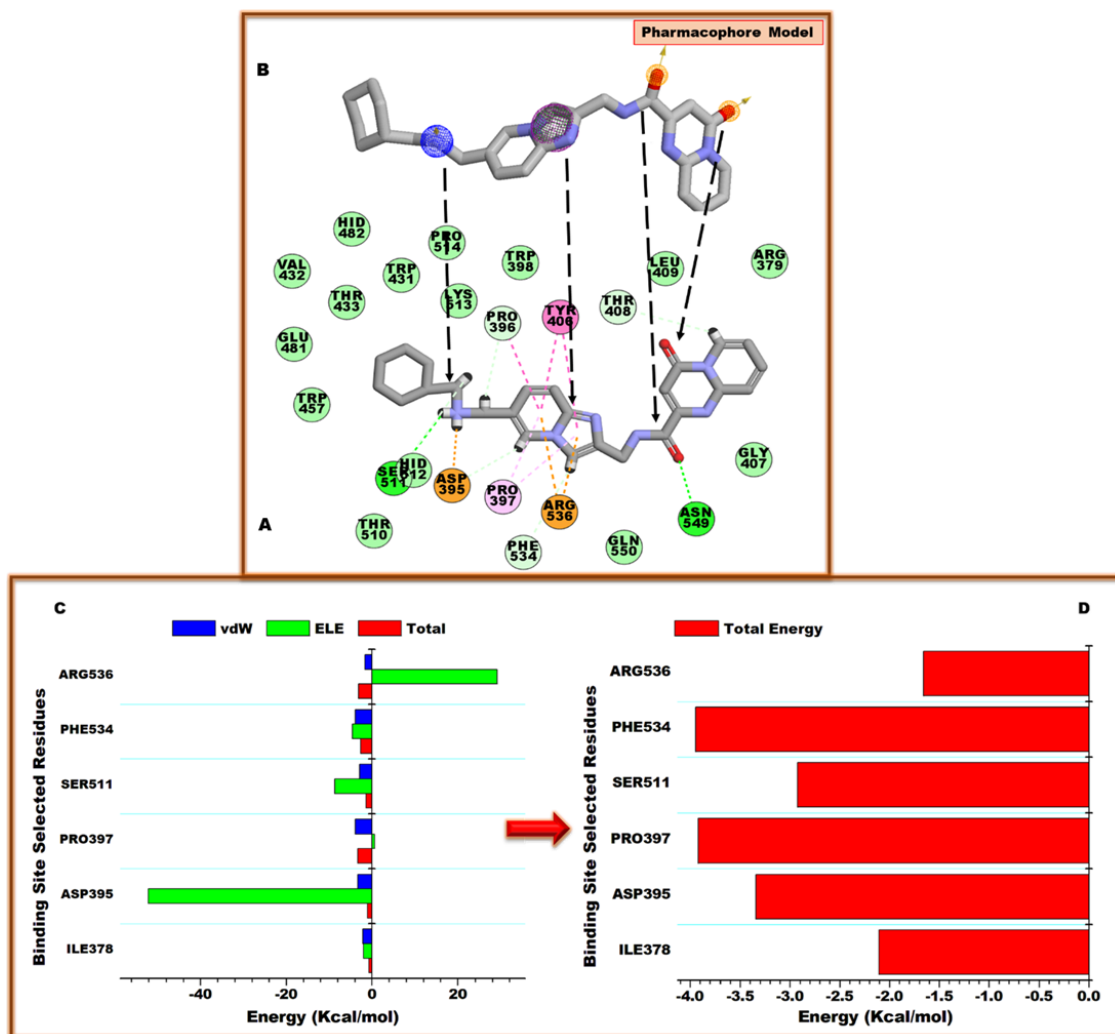
Figure 5

(A) 2D representation of the interactions of V22 with the energy-contributing residues. (B) Pharmacophore model (V22), 3D indicating features and amino acids most frequently participated in the ligand-receptor interaction and was used to develop a virtual screening model based on the METTL3-V22 complex. Dotted black arrows showed the hydrogen acceptor components, aromatic, hydrophobic components, hydrogen donor, and lastly, the positive ion. (C) Energy plots of high energy contributing residues. (D) Total energy contribution plots of the residues crucial in the pharmacophore modeling.
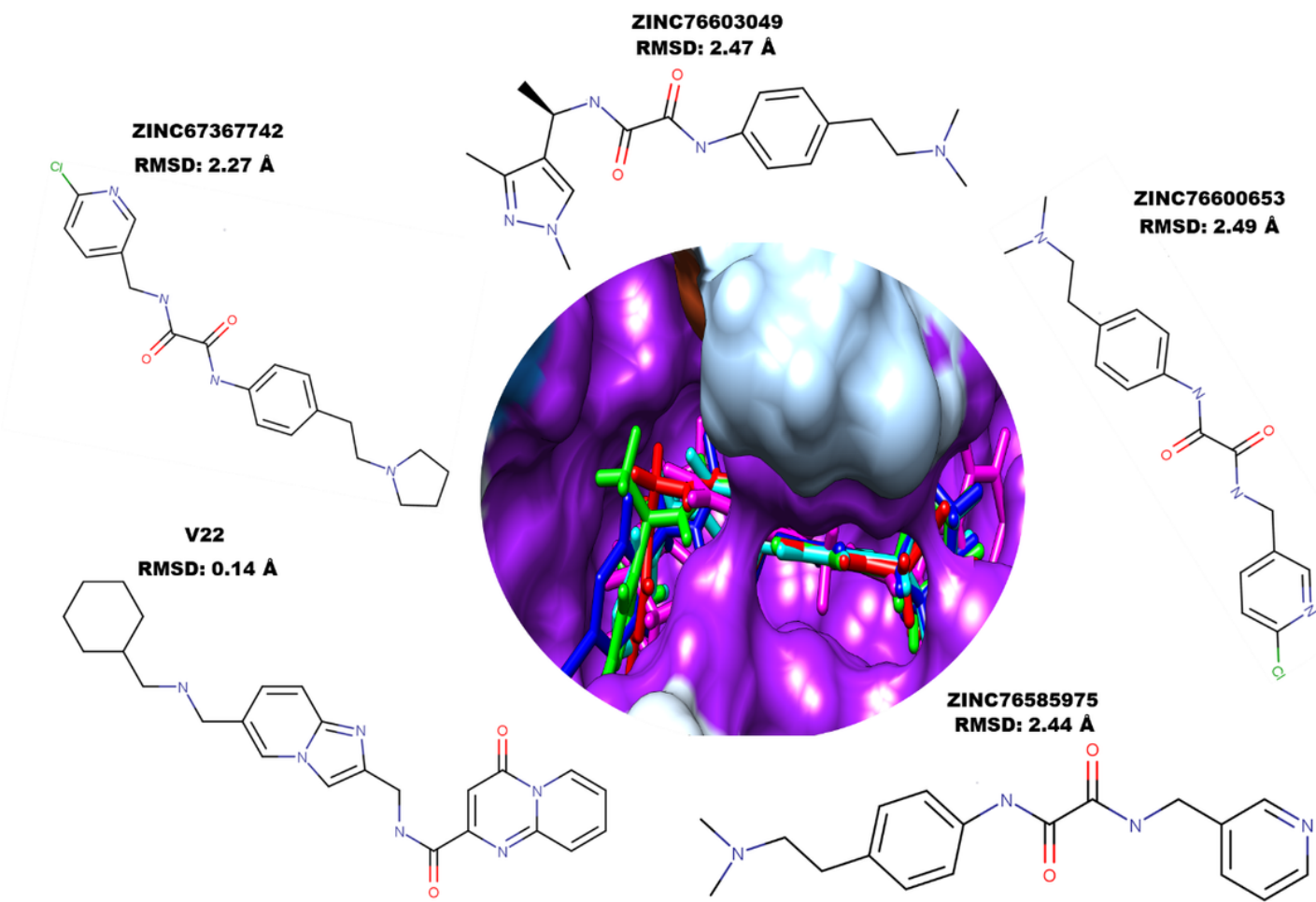
Figure 6

2D structures of the selected compounds and the RMSD values of their poses in comparison to V22 after docking.
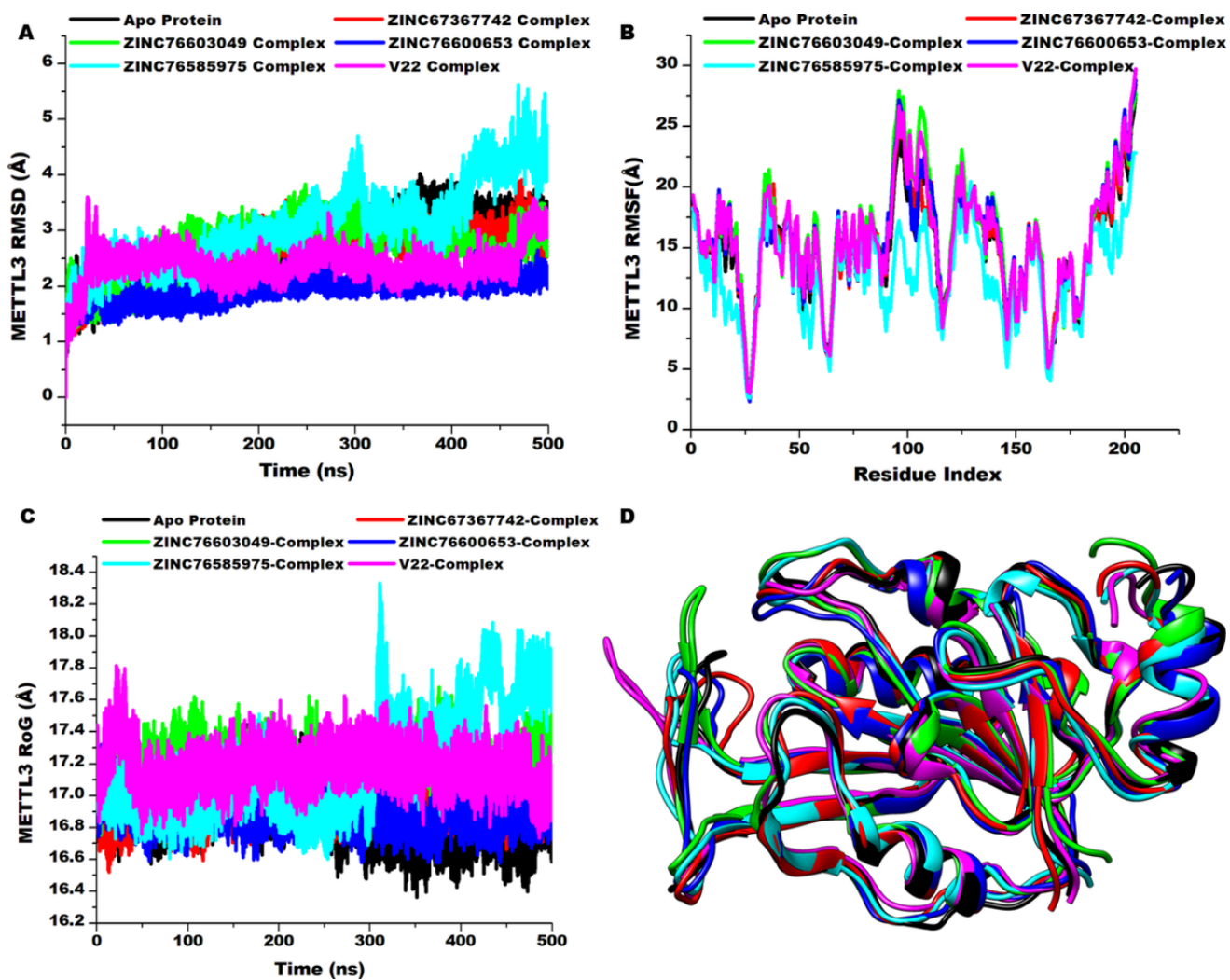
Figure 7

(A) RMSD plot of C$_\alpha$ atoms, (B) comparative RMSF plot of single residues, (C) comparative plot RoG plot, and (D) the superimposed METTL3 of the unbound apo (black) in comparison with V22-METTL3 (magenta), ZINC67367742-METTL3 (red), ZINC76603049-METTL3 (green), ZINC76585975- METTL3 (cyan), and ZINC76600653- METTL3 (blue).
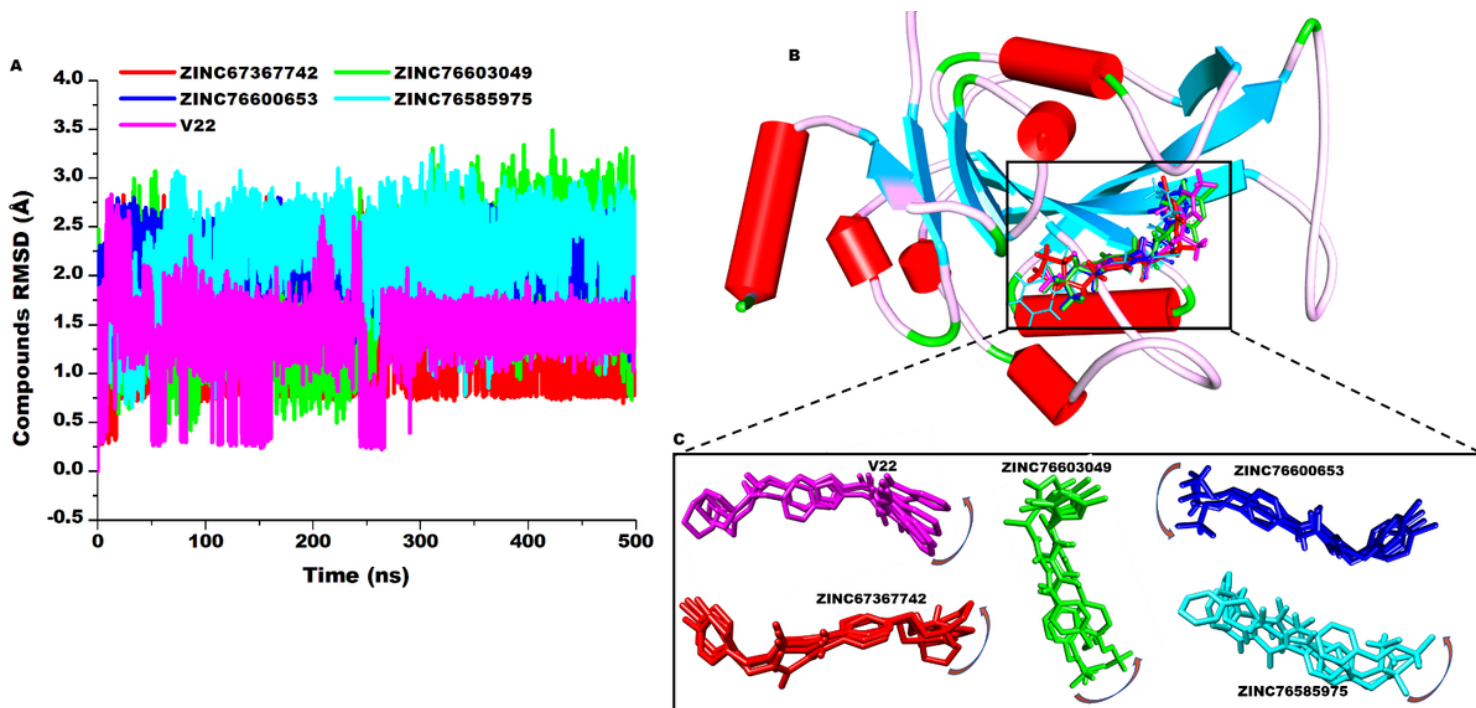
Figure 8

(A) Comparative RMSD plot of the hit compounds and V22 throughout the simulation. (B) structure of METTL3 in complex with the compounds and V22. (C) orientations of the compounds over the simulation period.
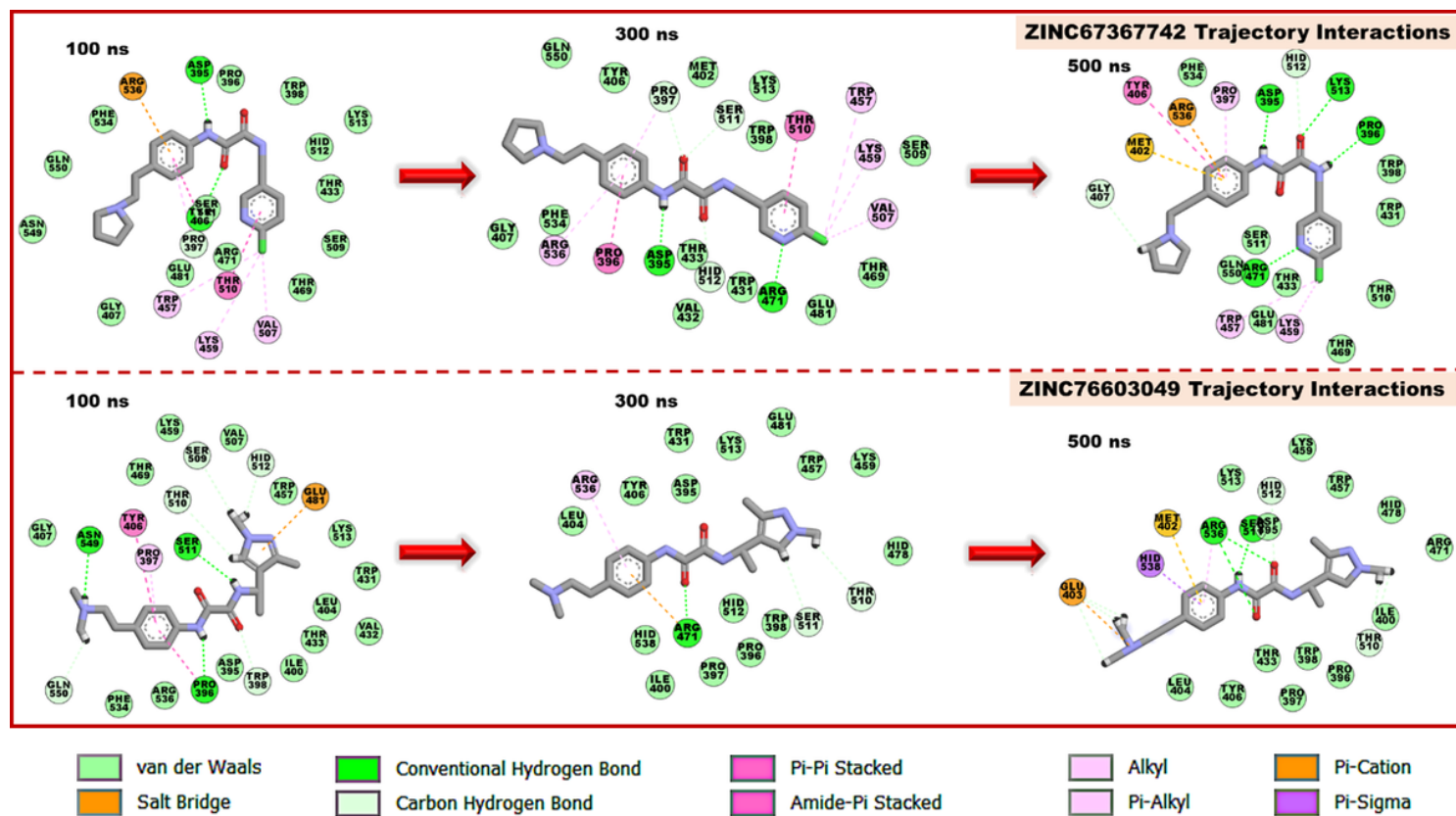

Figure 9

Interaction trajectories of ZINC67367742 and ZINC76603049 hit compounds over 100 ns, 300 ns and 500 ns.
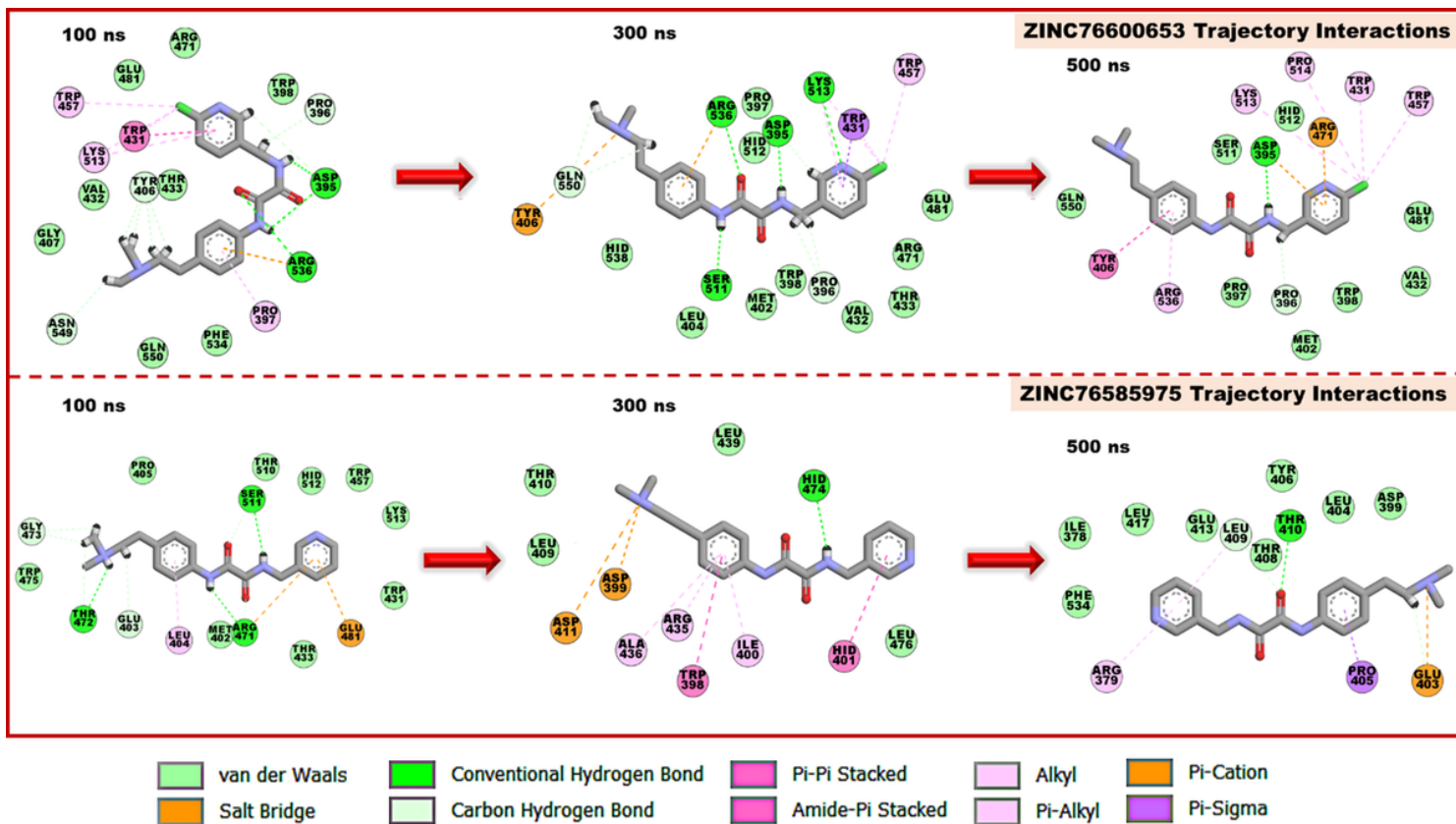
Figure 10

Interaction trajectories of ZINC76585975 and ZINC76600653 over the MD simulation period of 100 ns, 300 ns, and 500 ns.